

Article

Comparative Study of Groundwater-Induced Subsidence for London and Delhi Using PSInSAR

Vivek Agarwal ^{1,*}, Amit Kumar ², David Gee ³, Stephen Grebby ¹, Rachel L. Gomes ¹ and Stuart Marsh ¹

¹ Faculty of Engineering, University of Nottingham, Nottingham NG7 2RD, UK; stephen.grebby@nottingham.ac.uk (S.G.); rachel.gomes@nottingham.ac.uk (R.L.G.); stuart.marsh@nottingham.ac.uk (S.M.)

² School of Geography, University of Nottingham, Nottingham NG7 2RD, UK; amit.kumar@nottingham.ac.uk

³ Terra Motion Limited, Ingenuity Centre, Nottingham NG7 2TU, UK; david.gee@terramotion.co.uk

* Correspondence: vivek.agarwal@nottingham.ac.uk; Tel.: +44-743-6035-061

Abstract: Groundwater variation can cause land-surface movement, which in turn can cause significant and recurrent harm to infrastructure and the water storage capacity of aquifers. The capital cities in the England (London) and India (Delhi) are witnessing an ever-increasing population that has resulted in excess pressure on groundwater resources. Thus, monitoring groundwater-induced land movement in both these cities is very important in terms of understanding the risk posed to assets. Here, Sentinel-1 C-band radar images and the persistent scatterer interferometric synthetic aperture radar (PSInSAR) methodology are used to study land movement for London and National Capital Territory (NCT)-Delhi from October 2016 to December 2020. The land movement velocities were found to vary between -24 and $+24$ mm/year for London and between -18 and $+30$ mm/year for NCT-Delhi. This land movement was compared with observed groundwater levels, and spatio-temporal variation of groundwater and land movement was studied in conjunction. It was broadly observed that the extraction of a large quantity of groundwater leads to land subsidence, whereas groundwater recharge leads to uplift. A mathematical model was used to quantify land subsidence/uplift which occurred due to groundwater depletion/rebound. This is the first study that compares C-band PSInSAR-derived land subsidence response to observed groundwater change for London and NCT-Delhi during this time-period. The results of this study could be helpful to examine the potential implications of ground-level movement on the resource management, safety, and economics of both these cities.

Citation: Agarwal, V.; Kumar, A.; Gee, D.; Grebby, S.; Gomes, R.L.; Marsh, S. Comparative Study of Groundwater-Induced Subsidence for London and Delhi Using PSInSAR. *Remote Sens.* **2021**, *13*, 4741. <https://doi.org/10.3390/rs13234741>

Academic Editor: Nicola Cenni

Received: 29 September 2021

Accepted: 19 November 2021

Published: 23 November 2021

Publisher's Note: MDPI stays neutral with regard to jurisdictional claims in published maps and institutional affiliations.



Copyright: © 2021 by the authors. Licensee MDPI, Basel, Switzerland. This article is an open access article distributed under the terms and conditions of the Creative Commons Attribution (CC BY) license (<https://creativecommons.org/licenses/by/4.0/>).

Keywords: PS-InSAR; Sentinel-1; surface subsidence; groundwater; London; NCT-Delhi

1. Introduction

Water is essential to sustain life on earth; however, its availability is not uniform within the spatial and temporal domains. Groundwater meets a large part of the water demand, and ever-increasing dependence on this resource has led to groundwater depletion across various parts of the world [1–3]. Amidst the threat of global warming and climate change, groundwater acts as a lifeline for many parts of the world. Thus, adequate management of groundwater is essential to ensure its sustainability. Excessive abstraction and change in rainfall patterns make it necessary to regularly revise and monitor groundwater abstraction policies.

For decades, groundwater has been extensively exploited in aquifers for domestic, agricultural, and industrial purposes; this has necessitated subsequent artificial recharge to balance the groundwater depletion and control land subsidence [4,5]. Long-term groundwater exploitation and recharge in confined aquifers alters the piezometric and pore pressures in aquifers [6,7]. According to the effective-stress principle, aquifer systems consolidate owing to these changes in their properties, leading to land subsidence

[8,9]. Therefore, it is necessary to understand land subsidence and the compaction process caused by groundwater exploitation and recharge.

Extraction or recharge of groundwater can cause land subsidence or uplift, respectively, and this can cause significant harm to buildings, infrastructure, and the water storage capacity of aquifers [10–14]. The conventional methods to study land movement, such as global positioning systems (GPS), global navigation satellite systems (GNSS), levelling, and others, can provide precise information but are labour intensive, costly over vast extents, and have a poor resolution, and thus, an alternative is needed. Satellite interferometric techniques, such as persistent scatterer interferometric synthetic aperture radar (PSInSAR), provides the means for less tedious, cost-effective, large spatial coverage (basin level) mapping of ground movement without compromising on accuracy and precision [15–18]. This technique was first introduced by Alessandro Ferretti in 2000 [19] and has been developed and applied for mapping surface deformation associated with groundwater change [14,20–23]. While PSInSAR can provide accurate land deformation information, it can only be calculated on permanent scatterers that maintain stable scattering with respect to time. This methodology is thus most effective in urban areas where multiple permanent scatters can be obtained [19].

The chalk is the most important aquifer unit in the English capital city of London and has been supplying water for public consumption since the 19th century [24]. London witnessed groundwater depletion during the first half of the 20th century, due to increased urban development and human activities. This depletion resulted in a decrease in groundwater level to 88 m below mean sea level (MSL) in the 1960s. The depletion was checked because of de-industrialisation in the 1980s, which led to groundwater rebound by 3 m/year in the 1990s. This dramatic rebound posed potential harm to buildings and structures and, to counter this, the General Aquifer Research, Development, and Investigation Team (GARDIT) strategy was implemented in 1992 [25]. This enforced licensed groundwater withdrawal and regular monitoring and thus stabilised the groundwater around the year 2000, and since then, groundwater has been monitored regularly.

India is home to over 1.3 billion people, and its ever-increasing population, urbanisation and non-uniform abstraction have likewise increased the depletion rate of groundwater resources [26]. The National Capital Territory (NCT) of Delhi lies in the heart of India and forms the capital city of the country. The subsurface geological features of NCT-Delhi determine its discrete landform units, which are directly related to groundwater availability. The primary source of irrigation in NCT-Delhi is groundwater, although surface water is also available from Trans Yamuna Canal Network. The Central Ground Water Board (CGWB) monitors and publishes groundwater records for India. It took on the aquifer mapping program during the 12th five-year plan for the entire country (including NCT-Delhi) for sustainable development and management of groundwater resources [27]. The groundwater level in NCT-Delhi is continuously declining and is at a critical stage [28], and this decline in groundwater level poses a significant threat of land subsidence [29].

The population explosions in London and NCT-Delhi exert increased pressure on groundwater resources, thus posing a threat of land subsidence. However, the subsurface geology and infrastructure of the two cities are different, and yet the responses of groundwater to anthropogenic activities and its subsequent effect on land movement is not well understood. To the best of our knowledge, no previous attempts have been made to simultaneously examine the specific causes of groundwater-induced land subsidence for London alongside that of NCT-Delhi using PSInSAR. In this study, the groundwater-induced land subsidence for the two major cities is studied between October 2016 and October 2020 using a variety of geospatial techniques such as PSInSAR, GIS, spatio-temporal analysis, mathematical modelling, and statistical analysis. The objectives of this paper are (i) to describe spatio-temporal variation in land subsidence/uplift and investigate the natural and anthropogenic factors affecting land deformation; (ii) to analyse localised uplift, subsidence, and differential movement; (iii) to study temporal and spatial variation in groundwater and related subsidence at different locations for both the cities; and (iv) to

construct a mathematical model where a groundwater change input could be used to calculate the expected localised change in land deformation.

2. Study Area

The geographical areas selected in this study are the administrative area of Greater London (Figure 1a) and the administrative area of NCT-Delhi (Figure 1b). London extends over $0^{\circ}30' W$ to $0^{\circ}20' E$ longitudes and $51^{\circ}42' N$ to $51^{\circ}17' N$ latitudes, comprising nearly 1600 km^2 in the southern part of England. Meanwhile, the NCT-Delhi area is bounded by $76^{\circ}50'24'' E$ to $77^{\circ}20'30'' E$ longitudes and $28^{\circ}24'15'' N$ to $28^{\circ}53'00'' N$ latitudes, comprising a 1500 km^2 area in the central part of India.

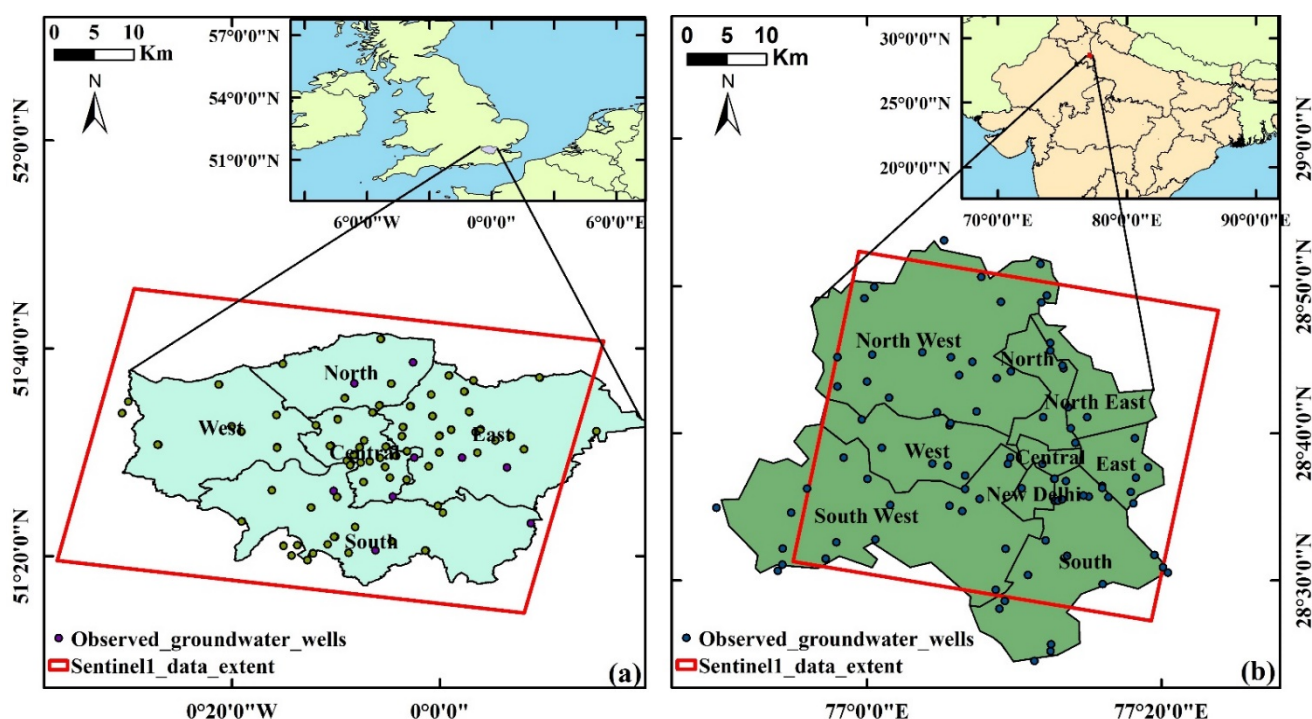


Figure 1. Study area showing administrative boundary of (a) London and (b) NCT-Delhi. The red boundary shows the extent of Sentinel data processed, and black dots show the location of observed groundwater wells.

The London basin is infilled by younger Paleogene deposits, and the chalk group forms a rim around it and has a depth exceeding 200 m in central London [30,31]. The NCT-Delhi is bounded by the Indo-Gangetic plains on the north-eastern side, Aravalli ranges on the southern side, and Indian Thar desert on the western side. It is drained by the Yamuna sub-basin, which flows in a north–south direction. The NCT-Delhi is dominated by three main geomorphic units: rocky surface, older alluvium plain, and flood plains of Yamuna. The area has mainly calcareous soil and comprises clay, silt, and fine to medium sand [28].

In the United Kingdom (UK), chalk aquifers account for about 60% of the groundwater used [32], and provide approximately 80% of the water supply in the River Thames catchment and 20% in London alone [33]. In NCT-Delhi, the groundwater level variation is quite extensive because of the wide range of topographic relief. The southern part of NCT-Delhi has deeper wells ($\sim 40 \text{ m}$ below ground level) compared to those in the northern part ($\sim 10 \text{ m}$ below ground level) [34]. In both cities, the local hydrogeological conditions mainly govern the groundwater conditions, and it is controlled by a mix of rainfall, river, canal water, and irrigation return flows.

The population of London had an increased rate of 1.4% per annum during the decade 2001–2011, while the rate for NCT-Delhi was 2.25%. The official projected population for London in 2025 is 9.31 million [35], while that for NCT-Delhi is 22.1 million [36]. These

estimates represent the urban agglomeration of the city, which typically includes the city's population in addition to adjacent suburban areas.

London's climate is warm and temperate, and the average annual temperature and the average annual rainfall is 11.1 °C and 621 mm, respectively. At the same time, NCT-Delhi is characterised by extreme dry hot summer and extreme cold winter climatic conditions. The temperature varies from a minimum of 7.3° in winter to a maximum of 47° in summer and receives a mean annual rainfall of 611.8 mm. The land use within both cities is dominated by dense to medium density urban fabric with multiple industrial units.

The demography, geology, rainfall, and hydrology of London and NCT-Delhi are highly contrasting. The two cities represent densely populated urban cities of developed and developing nations, respectively, and land deformation problems have been reported in both these cities. This study will help to improve the knowledge of land deformation response to groundwater use, through seeking to establish whether the land deformation response to groundwater change is universal irrespective of the differences in the characteristics of the cities, or whether it is very much location specific. This outcome of the study could therefore contribute towards infrastructure planning of urban areas in developed and developing nations.

3. Materials and Methods

3.1. PSInSAR Processing

The data specifications and overall methodology used in this study are summarised in Table 1 and Figure 2, respectively. Land movement for each study area was calculated using the PSInSAR principle [19] implemented in the ENVI SARscape software [37]. The software package is highly efficient at interferometric synthetic aperture radar (InSAR) processing using DInSAR, PSInSAR, and SBAS InSAR techniques, and supports all the latest synthetic aperture radar (SAR) sensors [38–40]. The PSInSAR technique, in general, requires at least twenty or more SAR image pairs to generate reliable results [17]. Specifically, stacks of 99 and 95 Sentinel-1 C-band images acquired between October 2016 and October 2020 over London and NCT-Delhi, respectively, were obtained and used to compute land movement.

Table 1. Data and software used.

Data	London	NCT-Delhi
InSAR Data	99 Sentinel-1 SLC images	95 Sentinel-1 SLC images
	VV polarisation, Frame 422, Descending, IW Beam mode	VV polarisation, Frame 496, Descending, IW Beam mode
	Resolution: Azimuth: 20 m by Range: 5 m	Resolution: Azimuth: 20 m by Range: 5 m
	Repeat Cycle: 12 days	Repeat Cycle: 12 days
	Wavelength: 5.6 cm, C-band	Wavelength: 5.6 cm, C-band
	Master Image: 1 November 2018	Master Image: 24 September 2018
	Time period: October 2016 to October 2020	Time period: October 2016 to October 2020
Digital Elevation Model: SRTM V4	Digital Elevation Model: SRTM V4	
Software Used: ENVI SARscape, ArcGIS (ArcMap 10.2.2)	Software Used: ENVI SARscape, ArcGIS (ArcMap 10.2.2)	
Ancillary data	Borehole groundwater data from the UK Environment Agency for 81 boreholes.	Groundwater level data (Source: Central Ground Water Board, CGWB) for 98 boreholes. Geological data of Delhi (Source: CGWB)

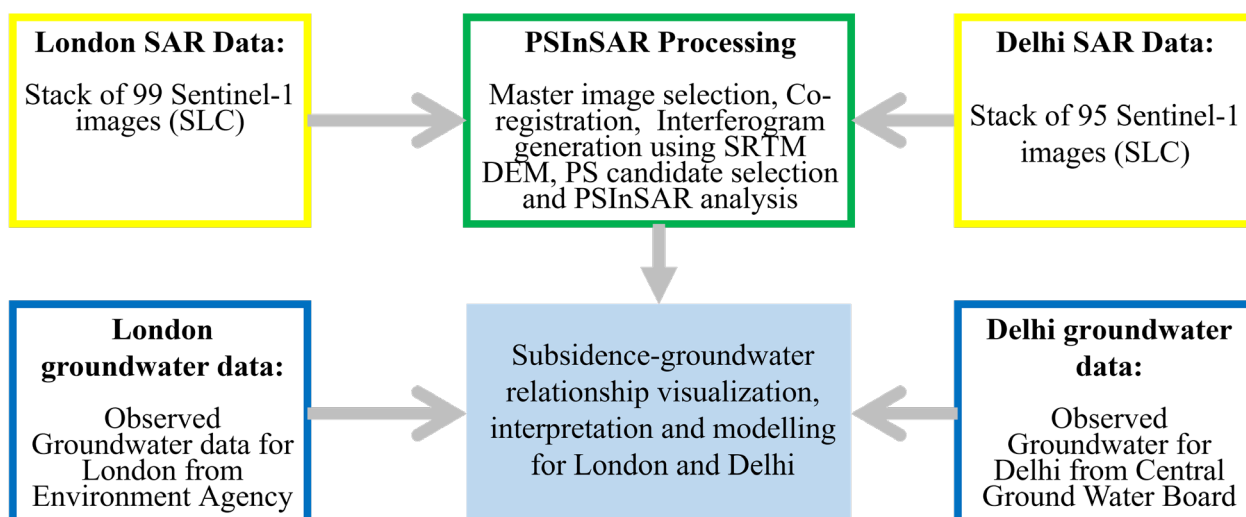


Figure 2. Methodology.

The SARscape module facilitates PSInSAR processing of SAR data in a multi-step, semi-automated process [41]. To begin, a master image is chosen to which all slave images are co-registered. To select the master image, the least average baseline of the stack is considered so that an optimum spatio-temporal position of the master image is ensured with respect to the slave images. This ensures increased coherence and better data co-registration, as small baselines are less sensitive to volume de-correlation [37,41]

After co-registration, interferograms were generated using master–slave pairs and flattening was achieved by applying a reference digital elevation model (SRTM DEM V4). To select a reference point for PSInSAR analysis, SARscape breaks the whole area into subsets (accounting for an overlap) if the area under consideration is bigger than a chosen threshold area. Then, each subset was analysed independently, with each having its own reference point. This was performed in order to improve the accuracy of the atmosphere estimation, and finally all the independent areas were mosaicked. This chosen threshold area is known as “Area for Single Reference Point (sq km)” [37]. In this study, this threshold was set at 25 km² and in total there were 238 subsets for London and 143 subsets for NCT-Delhi.

The density of permanent scatterers (PS), used to derive land motion measurements, relies on the selected coherence threshold for the PSInSAR analysis. The greater the coherence threshold, the better the quality and smaller the number of PS obtained, and vice versa. Therefore, the coherence threshold should be selected such that an optimum trade-off is reached between the quality of PS points and the number of PS points selected. The first step inversion was carried out to obtain the coherence, displacement velocity, and residual topography. These results were further employed for flattening the complex interferograms. Then, the second inversion step was performed to address the atmospheric phase components of the linear model products arising from the first inversion. Finally, geocoding was performed to display maps of the average (linear) velocity and displacement time-series for the observed time-period.

3.2. Groundwater Variation

To compare and validate the PSInSAR-derived land movements with groundwater variations, observed groundwater monitoring data were obtained from the UK Environment Agency for London (from 81 boreholes) and CGWB for NCT-Delhi (98 boreholes). The UK Environment Agency publishes an annual report on ‘Management of the London Basin Chalk Aquifer’ and the groundwater data was extracted from maps of the water table given in reports for January 2017 and January 2020 [25,42]. Additionally, the monthly

groundwater level for the Battersea chalk borewell was obtained from the UK Environment Agency. For NCT-Delhi, the groundwater data provided by CGWB was obtained for November 2016 and November 2020. The groundwater levels from 2016 were subtracted from that of 2020 to find the change and then interpolated using the inverse distance weighting (IDW) interpolation method [43] to produce a groundwater change map covering the whole area. The groundwater maps were then subsequently analysed in comparison to the subsidence maps.

3.3. Groundwater-Subsidence Mathematical Model

A simple mathematical model was used to calculate the amount of strata compaction resulting from a reduction in the piezometric head. The adopted model was a modified version of that applied in the Europe-led TerraFirma project [10] and coalfields in Derbyshire and Nottinghamshire [44]. It is used in order to analyse the relationship between groundwater level and observed subsidence for London and NCT-Delhi.

This model was based on the effective stress principle proposed by Terzaghi [45], which calculates the land deformation (subsidence or uplift) with respect to groundwater change (decrease or increase). The model was treated as a homogeneous matrix, where the initial bed thickness (b_0) (m) was calculated as the depth from the surface to the groundwater level at the start of the modelling epoch. As a formation was laid down and subsequently overlain by more material, the geostatic pressure (p_0) increases. The geostatic pressure is resisted by a combination of the fluid pressure of the pore water (p_{w0}) and the intergranular (effective) stress (p_{s0}) within the rock matrix [46].

$$p_0 = p_{s0} + p_{w0} \quad (1)$$

For an unconfined aquifer, the geostatic pressure is divided as p_{s0} (60%) and p_{w0} (40%), and for a confined aquifer the geostatic pressure is divided as p_{s0} (75%) and p_{w0} (25%). The stress transfer from the fluid to rock matrix per unit change in the piezometric head is calculated at 10 kPa/m [47]. The geostatic pressure is calculated from the initial bed thickness (b_0) as:

$$p_0 = 10 * b_0 \quad (2)$$

The total difference in bed thickness (Δb), after an instantaneous change in effective stress (Δp_s), is calculated as a function of the coefficient of volume compressibility (m_v) and initial thickness (b_0) as:

$$\Delta b = m_v * \Delta p_s * b_0 \quad (3)$$

where (m_v) can be defined as a function of the coefficient of compressibility (a_v) and the initial void ratio (e_0).

$$m_v = \frac{a_v}{1 + e_0} \quad (4)$$

where (a_v) is the ratio of change in void ratio to effective stress

$$a_v = \frac{\Delta e}{\Delta p_s} \quad (5)$$

The initial void ratio and final void ratio (e_1) can be related as follows:

$$\Delta e = e_1 - e_0 = -c_c \log \left(\frac{p_{s1}}{p_{s0}} \right) \quad (6)$$

$$e_0 = \frac{n_o}{1 + n_o} \quad (7)$$

where (c_c) is compressibility index, and (n_o) in initial porosity.

The model was constructed in R programming, where the compaction of each layer (formation) was calculated using the above parameters and equations. The total amount

of compaction is the combined total of each formation compaction. Each of the formations was assumed to contain a homogeneous matrix, and each assigned an average density and initial porosity based upon sediment type and depth of burial [48]. For London, the initial thickness of each formation was estimated using the London Basin 3D model constructed using GSI3D [48]. For NCT-Delhi, it was obtained from the hydrogeological framework and groundwater management plan of NCT-Delhi [49]. It is a layer-cake model which assumes that each layer is uniform; thus, thickness and physical properties for each subsurface layer are considered the same for all the locations of London, and for NCT-Delhi (Table 2).

Table 2. Physical properties of sub-surface layers.

Location	Formation	Thickness (m)	Void Ratio	Porosity	Compression Index
Delhi	Clay and Kankar	160	0.65	-	0.045
	Silt and Kankar	45	0.55	-	0.0924
	Sand	20	0.45	-	0.00525
London	Lambeth Group	11.98	-	0.35	0.0025
	Thanet Sands	10.20	-	0.3	0.0015
	Chalk Group	201.09	-	0.55	0.001

4. Results

Figure 3a,b displays the land displacement velocity map for London and NCT-Delhi obtained using 95 and 99 Sentinel-1 SAR images, respectively. The movement of land in the direction of sensor (uplift) and away from the sensor (subsidence) is represented by positive (green colour) and negative values (red colour), respectively. Table 3 summarises the statistics of the deformation results obtained.

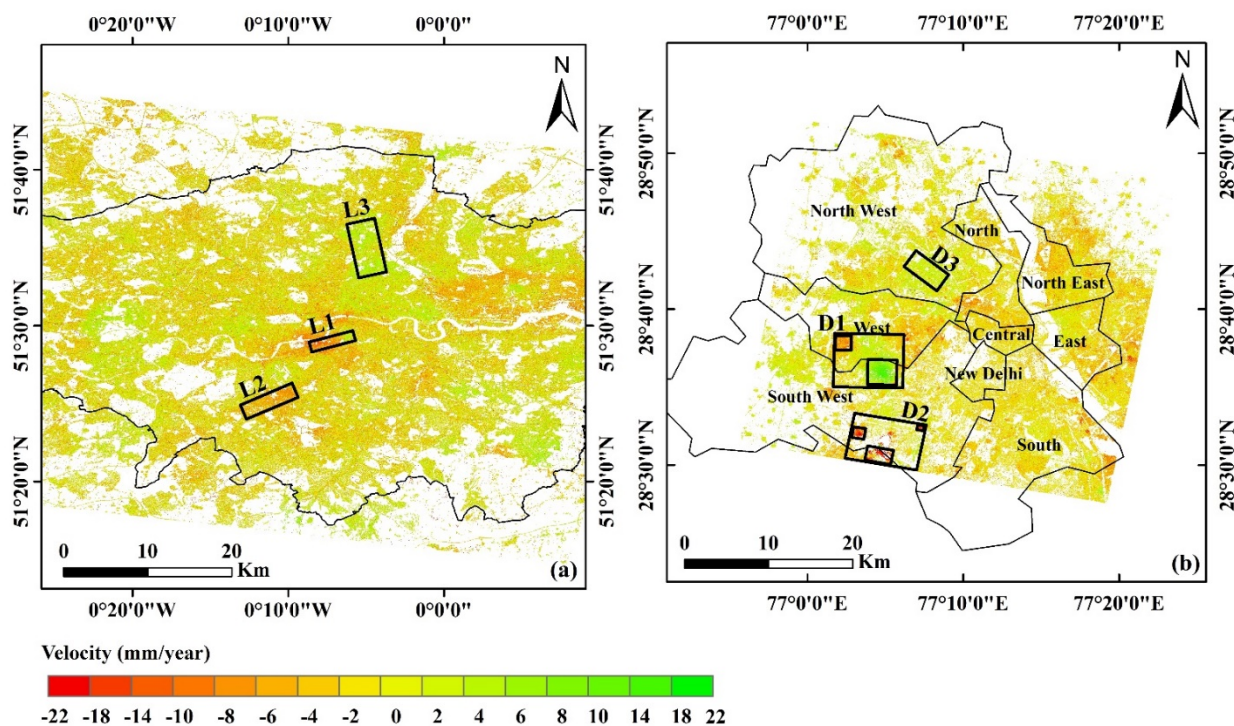


Figure 3. Land movement map obtained using Sentinel-1 data for (a) London and (b) NCT-Delhi. The green areas depict uplift, while the red areas depict subsidence. The black rectangular boxes show the selected sites for case studies.

Table 3. Statistics of PSInSAR-derived subsidence.

Area	Time-Period	Area (km ²)	PS Coherence Threshold Used	Number of Permanent Scatterers Obtained (PS)	PS Density (PS/km ²)	Mean Rate of Deformation (mm/year)	Standard Deviation (mm/year)
London	October 2016 to October 2020	2607	0.5	14,327,370	5496	−0.08	1.34
NCT-Delhi	October 2016 to October 2020	1611	0.5	7,764,180	4819	−0.04	1.70

Both London and NCT-Delhi are heavily built-up urban areas and therefore prove to be ideal sites for PSInSAR analysis. A coherence threshold of 0.50 was used for this experiment, resulting in a PS density of 2607 PS/km² for London and 1611 PS/km² for NCT-Delhi. For London, the land movement ranges between −24 and +24 mm/year, while for NCT-Delhi, it ranges from −18 to +30 mm/year. An area can typically be considered unstable if land movement is greater than ±10 mm/year [50]. For both these cities, even though the land movement is stable on the whole (in terms of the mean deformation rate shown in Table 3), it is predominantly spatially variable with distinct chunks of displacement in the form of either uplift or subsidence. Even though the land movement is small (mm-level), it is identifiable from the Sentinel data. These motions can likely be attributed to groundwater variations, underground construction activities, or subsurface geology, as discussed in Section 5.

For London, the groundwater data obtained from the Environment Agency report represents groundwater level in meters above ordnance datum (mAOD). For NCT-Delhi, groundwater measurements provided by the CGWB represent the depth to water level from the surface. In groundwater maps for both the cities, depletion is represented by red (negative values) and recharge by blue (positive values) (shown in Figures 4–9, explained in Section 5). The change in groundwater levels varies between −35 and +20 m for London and between −16 and +12 m for NCT-Delhi for the observed time-period (Tables 5–7, explained in Section 5).

Several interesting features are identified from the Sentinel PSInSAR measurements for both cities. These land movement features are discussed as case studies, the locations of which are marked with black rectangular boxes in Figure 3. These include:

- Differential land motion areas: Northern Line Extension, London (L1-a,b in Figure 4) and Magenta-Blue Metro Line, NCT-Delhi (D1-a,b in Figure 5).
- Subsidence areas: Wimbledon to Tooting, London (L2 in Figure 6) and Haryana-Delhi Border, NCT-Delhi (D2-a,b,c in Figure 7).
- Uplift areas: Bruce Castle to Abney Park, London (L3 in Figure 8) and Rohini, NCT-Delhi (D3 in Figure 9).

The results from the mathematical model used to compute the expected land movement from an observed change in groundwater level for all the case studies (L1, D1, L2, D2, and L3 and D3) are presented in Table 4. The 4-year average monthly change in the piezometric head is given for each case study. The average land movement at each location was calculated with this constant groundwater change rate. The land movement calculated at each location using the model and that calculated using PSInSAR is shown in Table 4. The difference in land deformation rate between the InSAR and modelled output is also shown. The mean of this difference in deformation for London is −0.63 mm/year with a standard deviation of 1.58, while that for NCT-Delhi is −0.55 mm/year with a standard deviation of 3.10 mm/year. The maximum and minimum difference in rate is 4.83 mm/year at D3 and 0.26 mm/year at L1-a, respectively.

Table 4. Comparison of land deformation from land subsidence and PSInSAR.

Area		Groundwater Monthly Change (m/month)	Model Change (mm/year)	PSInSAR Change (mm/year)	Difference in Rate (Model-PSInSAR)
L1	L1-a	-0.339	-3.18	-3.44	0.26
	L1-b	0.313	2.94	4.55	-1.61
D1	D1-a	-0.029	-7.79	-5.09	-2.7
	D1-b	0.038	10.14	11.06	-0.92
L2		-0.401	-3.75	-4.87	1.12
D2-a		-8.770	-8.77	-5.28	-3.49
D2	D2-b	-0.012	-3.19	-4.37	1.18
	D2-c	-0.022	-5.97	-3.74	-2.23
L3		0.145	1.36	3.64	-2.28
D3		0.041	11.13	6.30	4.83

5. Discussion

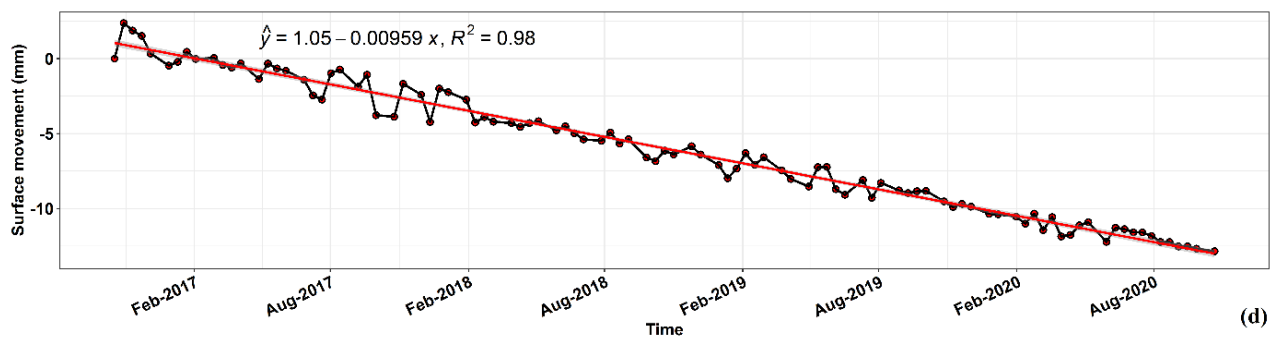
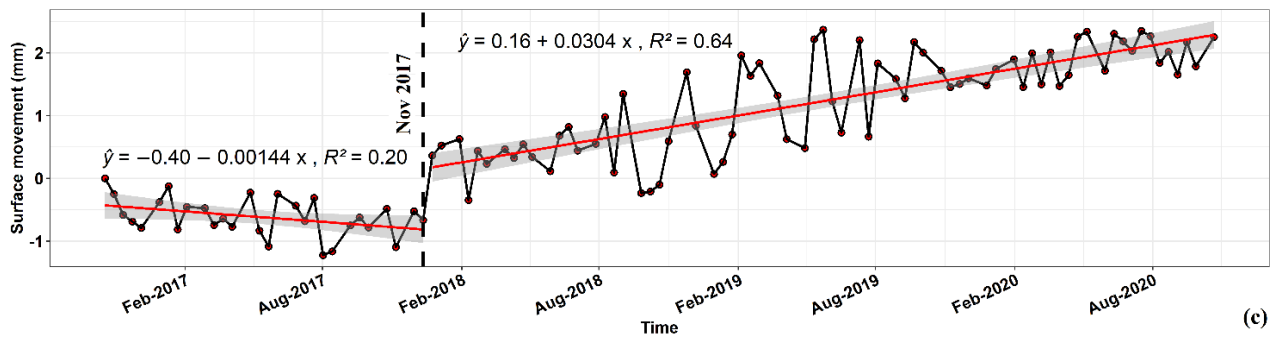
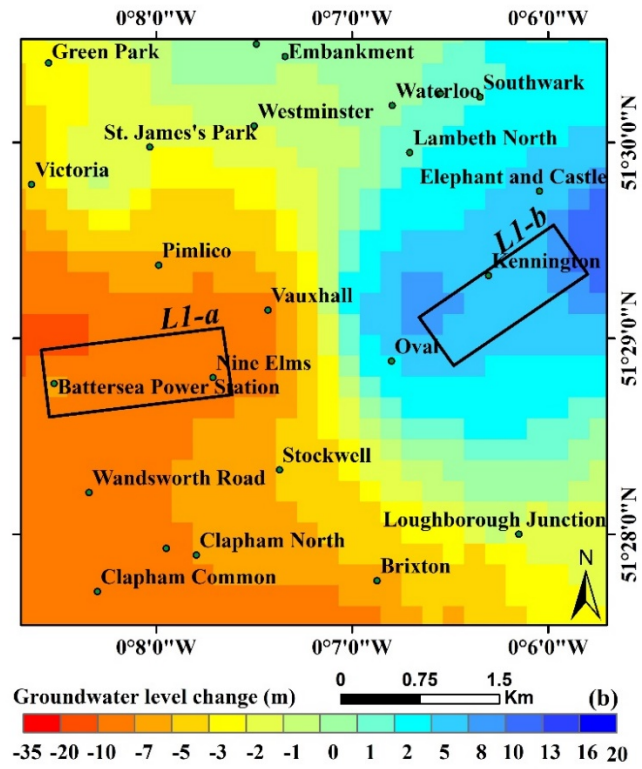
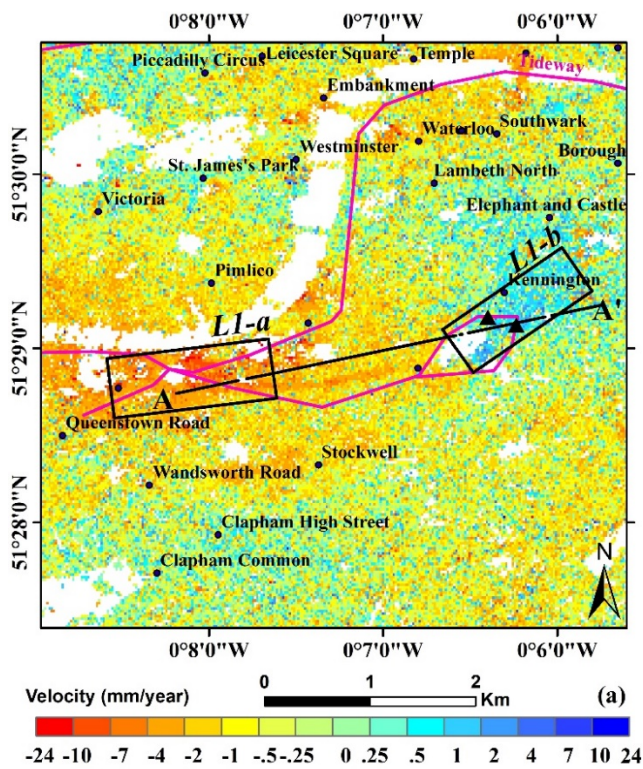
5.1. Differential Land Motion Areas

There are areas in London and NCT-Delhi where notable differential motion in the form of subsidence observed in close proximity to uplift occurs. In the London area, this is associated with the Northern Line extension (NLE) (Figure 4), while in the NCT-Delhi area, this is near the Janakpuri-Dwarka Magenta-Blue Line metro stations (Figure 5). Table 5 summarises the statistics of land movement and groundwater change for both areas.

Table 5. Statistics of land uplift and groundwater augmentation for Northern Line Extension (London) and Magenta-Blue Metro Line (NCT-Delhi).

Location ID	Location Name	Area (km ²)	No. of PS	PS Density (PS/km ²)	Land Deformation (mm/year)				Groundwater Change (m)		
					Max	Min	Mean	St. Dev.	Max	Min	Mean
L1-a	NLE: Battersea	0.68	7831	11,516	17.04	-22.71	-6.05	2.42	-9.40	-5.70	-8.15
L1-b	NLE: Kennington	0.54	6360	11,778	9.93	-10.26	4.55	1.37	10.61	6.20	7.52
D1-a	Magenta-Blue metro line: a	2.86	36,930	12,912	30.15	-18.49	-5.09	3.31	-2.32	-0.52	-1.38
D1-b	Magenta-Blue metro line: b	8.96	107,198	11,964	30.21	-18.69	11.06	4.61	+4.80	-1.16	+1.84

The NLE between Kennington and Battersea was proposed to help regenerate the Vauxhall, Nine Elms, and Battersea areas and is scheduled to be completed by the end of year 2021 [51]. Figure 4a shows the displacement velocity map obtained from Sentinel-1 images between October 2016 and October 2020. It highlights distinct subsidence and uplift pattern near Battersea Power Station and Kennington, respectively. To help analyse these patterns, the time series of surface deformation for both the uplifting and subsiding areas were also extracted (Figure 4c,d).



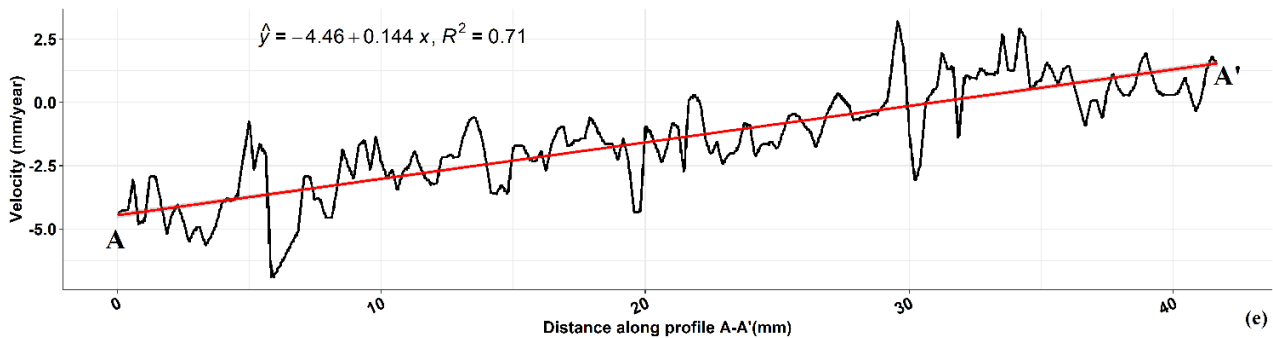


Figure 4. For Northern Line Extension: (a) PSInSAR land movement map, (b) groundwater change map, (c) time-series of land uplift (L1-b), (d) time-series of land subsidence (L1-a), and (e) profile across A-A' marked on (a). The black triangles in (a), represents the location of the two main dewatering shafts required for placing the tunnel boring machine.

The main tunnelling work of the NLE consisted of creating two tunnels between Battersea and Kennington Park. The construction for the NLE began in July 2016 [51] and required dewatering of the ‘deep’ aquifer, which includes the lower part of the Lambeth group. The dewatering shafts for the NLE are located on the northern edge of Kennington Park, and the location of the two main shafts required for placing the tunnel boring machines are shown in Figure 4a (black triangles). The geology of the area is relatively complex, with several faults, buried hollows and laterally discontinuous superficial strata [51].

The underground construction work, tunnelling shafts, and groundwater extraction contributed to the land motion pattern observed in this area. In Kennington, the average land motion trend during the observed time-period is that of uplift (Figure 4a), which is concurrent with the change in groundwater level (Figure 4b). However, the deformation time series exhibits phases of both subsidence and uplift during this period (Figure 4c). Specifically, the ground subsided during 2016–2017, before continuously uplifting since November 2017. This motion corresponds to subsidence due to dewatering during the construction of the tunnels, following by groundwater rebound (heave) once the dewatering ceased in November 2017. Around Battersea Power Station, the time series (Figure 4d) shows a linear trend of land subsidence between 2016 and 2020. The surface displacement here is consistent with the decrease in the groundwater level during this period (Figure 4b) and is most likely due to the groundwater abstraction that was undertaken to dewater the locality for the NLE tunnelling [51]. The construction activities around Battersea Power Station are still ongoing; hence, the groundwater extraction and associated ground deformation can be seen to continue beyond the observed time-period.

A strong displacement gradient between Battersea Power Station and Kennington Park can also be seen in the displacement profile A-A' (Figure 4e). It reveals that the area near the Battersea Power Station is experiencing subsidence of up to 6 mm (near A), which gradually decreases in magnitude along the profile. The motion is reversed, close to Kennington Park, with an uplift of >2 mm at point A'. There are numerous faults in this area within the chalks [25], which could potentially compartmentalise the aquifer and subsequently constrain the differential land movement within these segments.

Similar differential land movement can also be seen in NCT-Delhi in the area encompassing the Magenta-Blue Line metros (Figure 5a). The Blue Line metro is the longest metro line running on the Delhi metro network and was built in 2006 [52]. In Figure 5a, the area marked shows clear strong uplift sandwiched between Blue Line’s (phase 1) Janakpuri East to Dwarka Mor stations on the north-eastern side, and Dwarka sector 14 to Dwarka sector 10 stations on the south-western side. Moreover, the Magenta Line (line 8, phase 3), a rapid transit system, passes through the intense part of the uplift area, where the underground metro stations of Dabri Mor (South Janakpuri), Dashrathpuri, and Palam stations are located. Most of the underground construction for these stations was

completed by September 2016, and these then became operational in May 2018 [53]. De-watering in the area ceased at the end of 2016, and so the consistent uplift observed here most likely represents groundwater rebound.

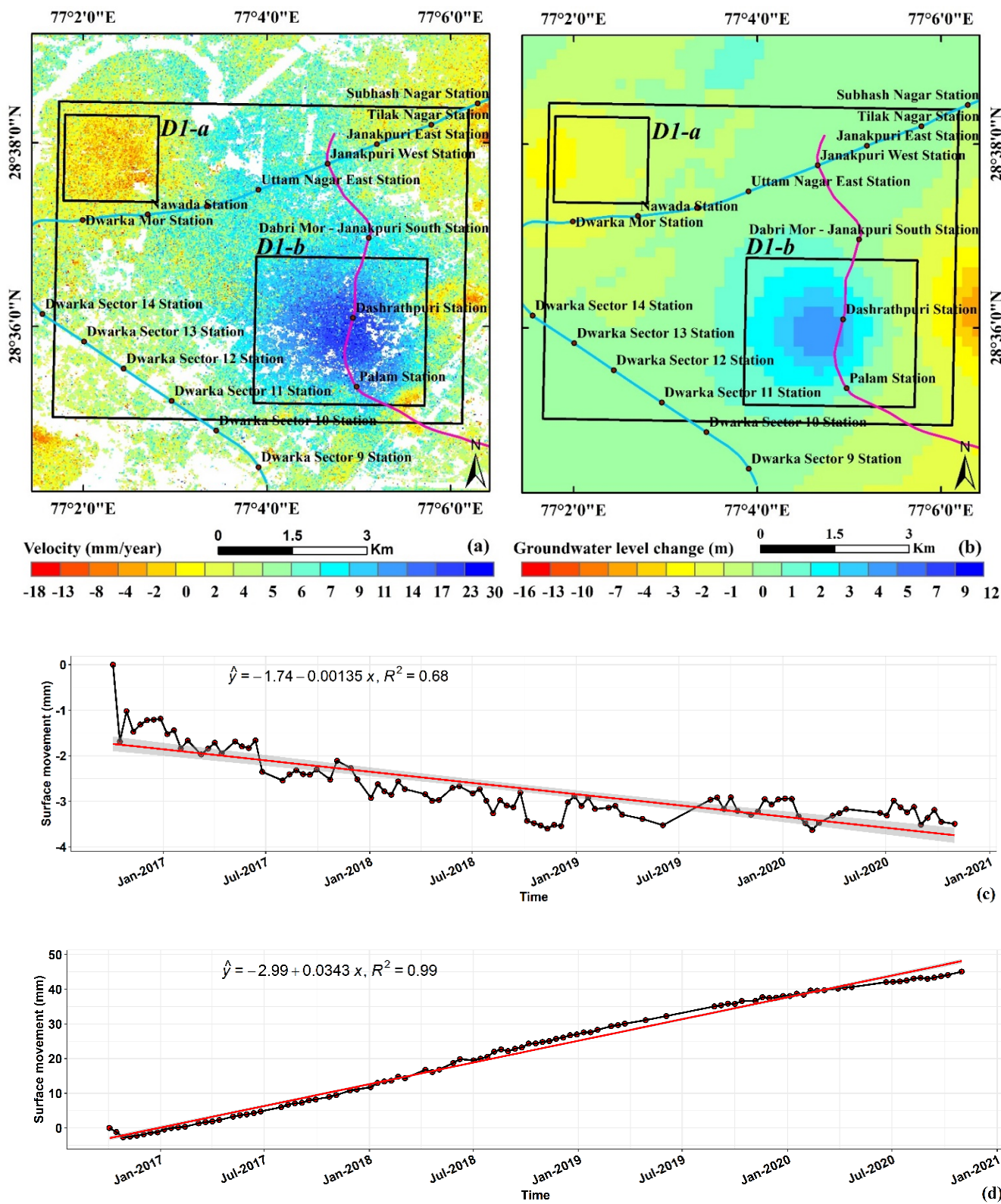


Figure 5. For Magenta-Blue metro line: (a) PSInSAR land movement map, (b) groundwater change map, (c) time-series of land subsidence (D1-a), and (d) time-series of land uplift (D1-b).

In Figure 5a, the area marked on the northwest (D1-a) is a heavily built-up area and contains buildings, roads, metro, temples, and other man-made structures. The area has an extent of 2.86 km² and contains 36,930 PS points. The average subsidence rate for the region is −5.09 mm/year. It includes the built-up urban areas of Laxmi Vihar, Ranjan Vihar, Shakti Vihar, Mahavir enclave, and important political buildings. The area also contains a densely packed residential complex, and consequently groundwater is extracted to meet the demands of the population, which could lead to subsidence [26]. The groundwater variation agrees with the observed subsidence pattern on visual inspection (Figure 5a,b). From Table 5, it can be seen that at L1-a, the average decrease in groundwater is 8.15 m, causing a resulting average subsidence of 6.05 mm/year. On the contrary at L1-b, the average increase in groundwater is 7.52 m, causing a resulting average subsidence of 4.55 mm/year

Clearly, both cities have a complex pattern of land movement, which depends on several factors, including natural processes such as compaction of deposits on the river floodplain and anthropogenic instability due to water abstraction and recent engineering works. The main cause of local land uplift was found to be groundwater rebound after completion of underground activities, whilst that for land subsidence was groundwater extraction. The relationship between ground motion rates and groundwater pumping showed good agreement for both cities, in a qualitative sense based on visual comparison of the maps (Figures 4 and 5), and in a quantitative sense based on the results in the Table 5.

5.2. Subsidence Areas

Areas where subsidence is dominant can also be seen in both London and NCT-Delhi. The London area extends from Wimbledon to Tooting (Figure 6), while NCT-Delhi area lies in the vicinity of Delhi-Haryana border (Figure 7). Table 6 summarises the statistics of land subsidence and groundwater depletion for both of these areas.

Table 6. Statistics of land subsidence and groundwater depletion for Wimbledon to Tooting (London) and Delhi-Haryana border (NCT-Delhi).

Location ID	Location Name	Area (km ²)	Number of PS	PS Density (PS/km ²)	Land Deformation (mm/year)				Groundwater Change (m)		
					Max	Min	Mean	St. Dev.	Max	Min	Mean
L2	Wimbledon to Tooting	7.71	86,822	11,261	22.89	−14.61	−4.87	1.19	−5.95	−13.79	−9.6
D2-a	Delhi-Haryana Border: a	1.65	13,444	8148	28.43	−18.71	−5.28	5.26	−9.46	−5.97	−7.77
D2-b	Delhi-Haryana Border: b	4.70	26,368	5610	30.19	−18.71	−4.37	7.71	−7.72	−4.87	−5.64
D2-c	Delhi-Haryana Border: c	0.40	4653	11,632	28.01	−18.71	−3.74	6.63	−1.46	−0.73	−1.06

In Figure 6a, the area marked (L2) is located in south London and mainly contains urban built-up areas, which comprise construction, roads, metros, residential complexes, and other man-made structures. The PSInSAR analysis of this area achieved a PS density of 11,261 PS/km², with an average subsidence rate of −4.87 mm/year. The linear regression of the time series for average land movement of the area (Figure 6c) has a negative slope (i.e., subsidence), with an R² value of 0.8. The area contains the urban centres of Tooting, Colliers, Dundonald Road, Wimbledon, and others. The London Clay Formation is predominant in the area, and clays, silt, and sand of the Lambeth group are also present in small deposits. More than 250 working borewells are present in the area [54], and the observed deformation pattern is mainly related to increased groundwater abstraction at

these locations. Figure 6b shows groundwater change between 2017 and 2020, which shows groundwater level changes in the range of -5.97 to -13.7 m. In this area, water is abstracted from chalk up to depth greater than 70 m, and the groundwater level was lowered by an average of 9.6 m during the observed time-period.

The northwest edge of the area is bounded by the Wimbledon Fault. In this area, it appears that faults parallel to the Wimbledon Fault are controlling the local subsidence patterns, and groundwater movement [10]. It is also noteworthy that the width of the Thames floodplain increases markedly downstream of the Wimbledon Fault, due to the outcrop of the Holocene deposits. The author in [55] found that ground motions in this area were attributed to groundwater abstraction from the Merton Abbey public water supply well (green triangle in Figure 6a,b) during 1995–2020. This was further analysed in the framework of the BGS Terrafirma project, via the production of the Terrafirma, London H3 Modelled Product [10]. The study found striking correlation between variation in land movement and groundwater change at the Merton Abbey public water supply well, where the groundwater level dropped by 30 m enforcing subsidence of 0.5 mm/year.

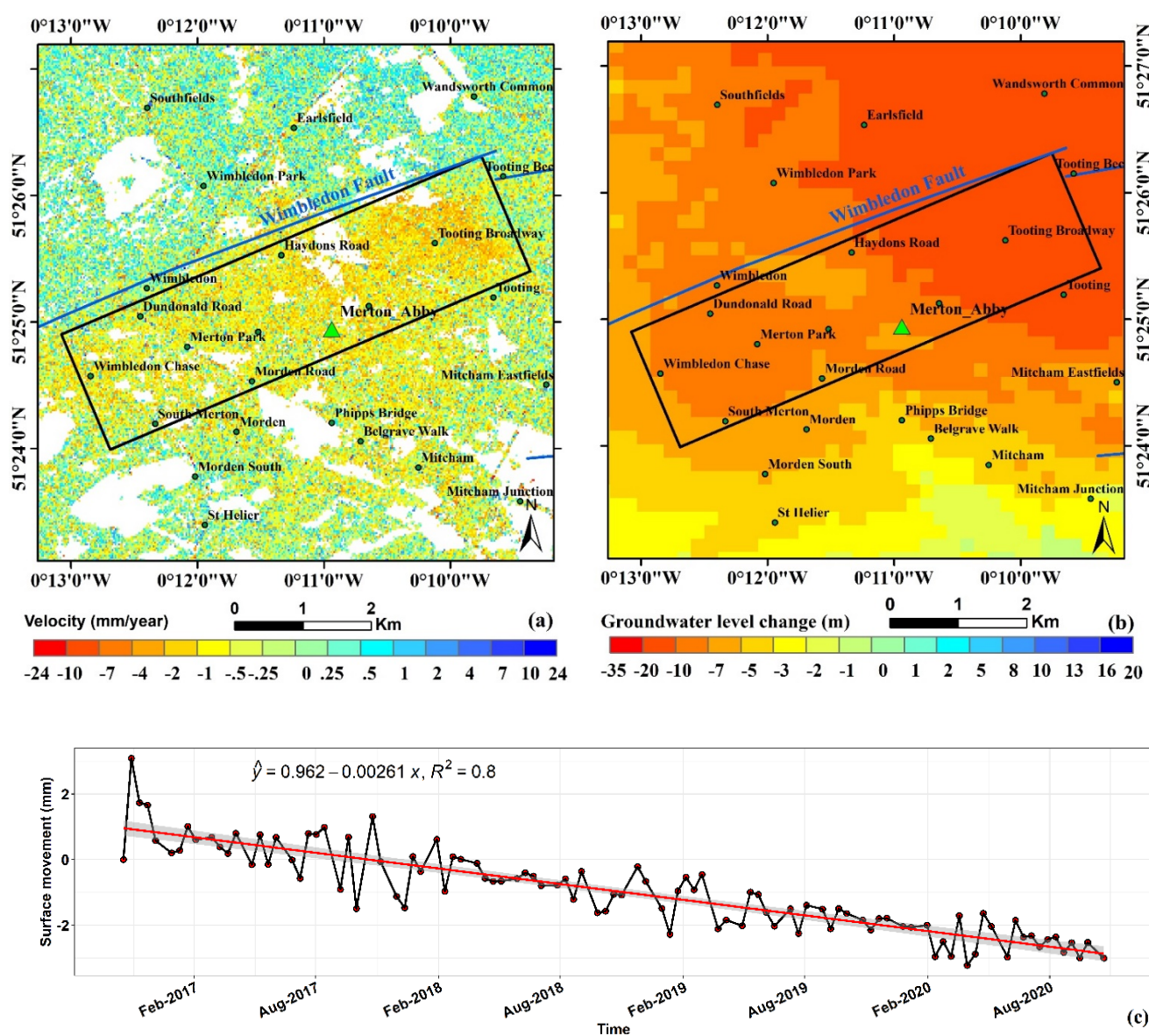


Figure 6. For Wimbledon to Tooting: (a) PSInSAR land subsidence map, (b) groundwater depletion map, and (c) time-series of land subsidence (L2). The green triangle in (a,b) shows the location of Merton Abbey public water supply well.

The Wimbledon-Tooting area contains numerous underground metro stations where groundwater extraction and construction activities are carried out for repair and maintenance work. In addition, the area extends over only 7.7 km² and has more than 250 active boreholes clearly indicating that groundwater depletion is evident in this area. These are the driving force for the subsidence pattern obtained, and groundwater depletion map is consistent with the subsidence map.

A similar subsidence pattern can be seen in the vicinity of Delhi-Haryana border marked in Figure 7a. The area, as a whole, lies to the south of Airport Express metro line joining New Delhi to Dwarka sector 21. All three metro stations shown on Figure 7a (Delhi Aerocity, IGI Airport, and Dwarka sector 21) are underground stations and opened in 2011 [52].

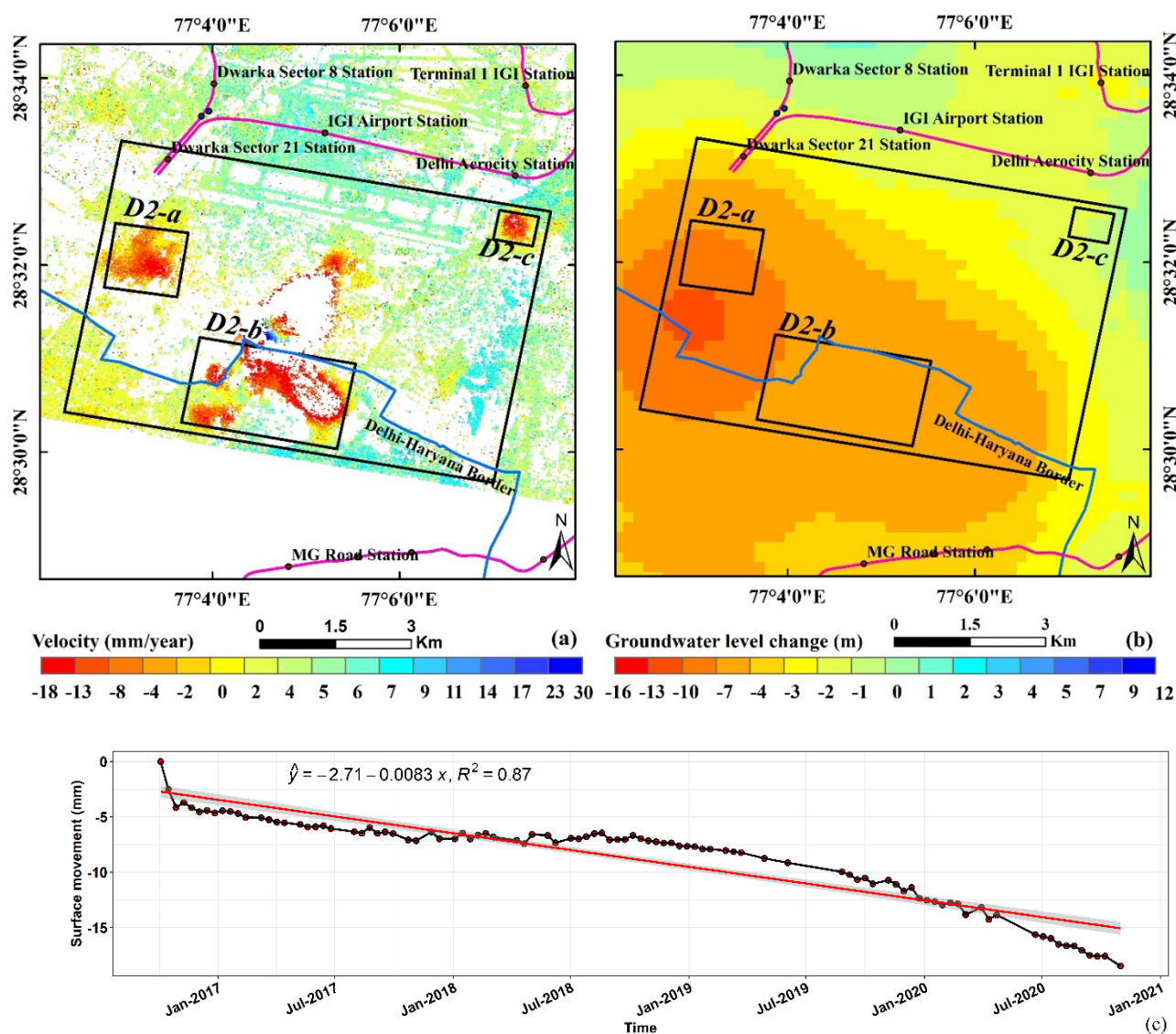


Figure 7. For Delhi-Haryana: (a) PSInSAR land subsidence map, (b) groundwater depletion map, and (c) time-series of land subsidence for the area (D2-b).

Additionally, the area under the three black boxes (D2-a, D2-b, and D2-c) in Figure 7a, are heavily populated areas with a high population density of 20,000 person/km² [56]. The area D2-b, has a large population living on the borders of Delhi-Haryana, as these people can use the benefits of a capital city without paying the heavy living expenses [57].

This increased population exerts heavy pressure on the groundwater resources and leads to groundwater depletion. The linear regression of the time series (Figure 7c) for average land movement of the study area (D2-b, in Figure 7a) has a negative slope (thus subsidence), with an R^2 value of 0.87. Moreover, continuous underground construction work is being carried out for extension of the metro lines [53]. The map of groundwater depletion (Figure 7b) is consistent with that of subsidence maps, and so it can be reasonably concluded that the two are directly interdependent. Overall, the subsidence pattern for both cities (London and NCT-Delhi) is similar and interestingly controlled by the same factors, despite differences in their bedrock geology.

5.3. Uplift Areas

The areas that experience notable uplift in London and NCT-Delhi are also evident. The London area stretches from Bruce Castle to Abney Park (Figure 8), while the NCT-Delhi area is across the Rohini metro line (Figure 9). Table 7 summarises the statistics of land uplift and groundwater change for both these areas.

Table 7. Statistics of land uplift and groundwater augmentation for Bruce Castle to Clissold Park (London) and Rohini (NCT-Delhi).

Location ID	Location Name	Area (km ²)	Number of PS	PS Density (PS/km ²)	Land Deformation (mm/year)				Groundwater Change (m)		
					Max	Min	Mean	St. Dev.	Max	Min	Avg
L3	Bruce Castle to Clissold Park	13.8	150,354	10,895	23.09	-20.54	3.64	1.21	8.28	-0.04	3.48
D3	Rohini	10.1	99,665	9867	29.49	-18.14	6.30	2.17	1.50	2.58	1.97

The area marked in Figure 8 is contains Holocene alluvium, and the uplift is observed due to groundwater rebound arising from aquifer recharge for an area of 13.8 km². The InSAR results show an uplift of 3.64 mm/year based on a PS density of 10,895 PS/km². The linear regression line for the time series (Figure 8c) shows a positive slope (i.e., uplift), with an R^2 value of 0.6. Visually, the groundwater change map is consistent with the land subsidence map. This area is a low-lying river flood plain with elevations between 2 and 14 mAOD. The bedrock geology is dominated by the London Clay formation, silt, and sand of the Lambeth Group, whereas superficial deposits in the area consist mostly of alluvium of the River Thames and River Lee. The area has several water reservoirs and recreation parks, which assists with the recharge of groundwater. The recreation parks include Clissold park, Abney park, Downhills park, Lordship recreation ground, and Bruce Castle park; and the reservoirs include East and West Reservoirs with Warwick and Lockwood reservoir in the area's vicinity [57]. Seepage from the various water reservoirs and artificial watering of the various recreation parks are the important contributing factors for the increase in groundwater level, which is likely attributable for the land uplift observed.

The area marked in Figure 9 shows the Rohini area, with the Red Line metro stations, which consists of the first stretch of the Delhi Metro. These stations were built in phase 1 Red Line and opened in 2004 [52]. Figure 9a shows the displacement velocity map obtained from Sentinel-1 PSInSAR analysis between October 2016 and October 2020 and reveals distinct uplift with an average rate of 6.30 mm/year. The groundwater variation map is visibly consistent with the pattern shown in the land deformation map, and the time series also confirms continuous uplift. This is one of the wealthiest areas of Delhi city and is subject to managed groundwater abstraction and recharge [58]. This has led to a rise in groundwater level and the subsequent continuous uplift.

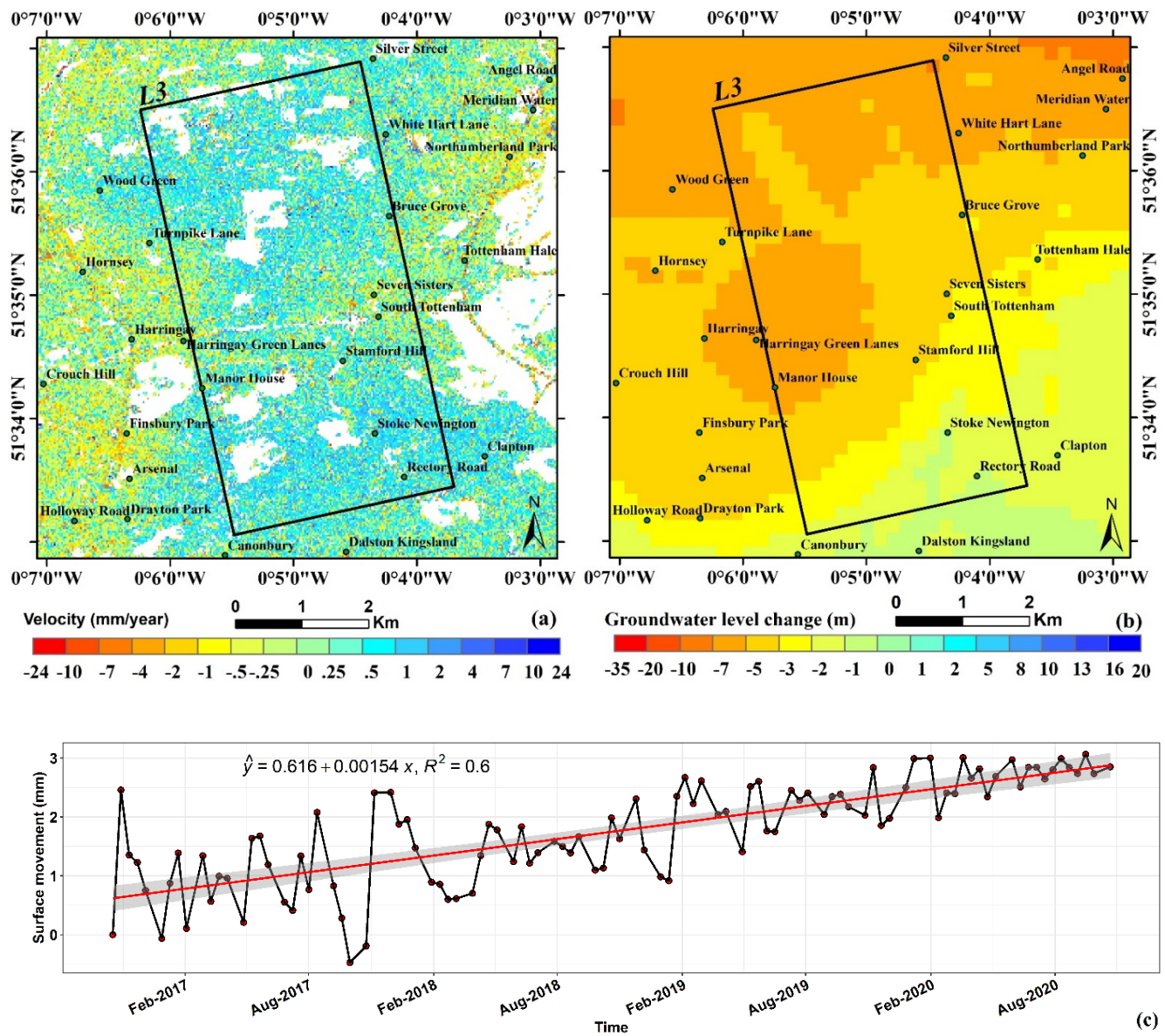


Figure 8. For Bruce Castle to Abney Park: (a) PSInSAR land uplift map, (b) groundwater augmentation map, and (c) time-series of land uplift for the whole area marked in box.

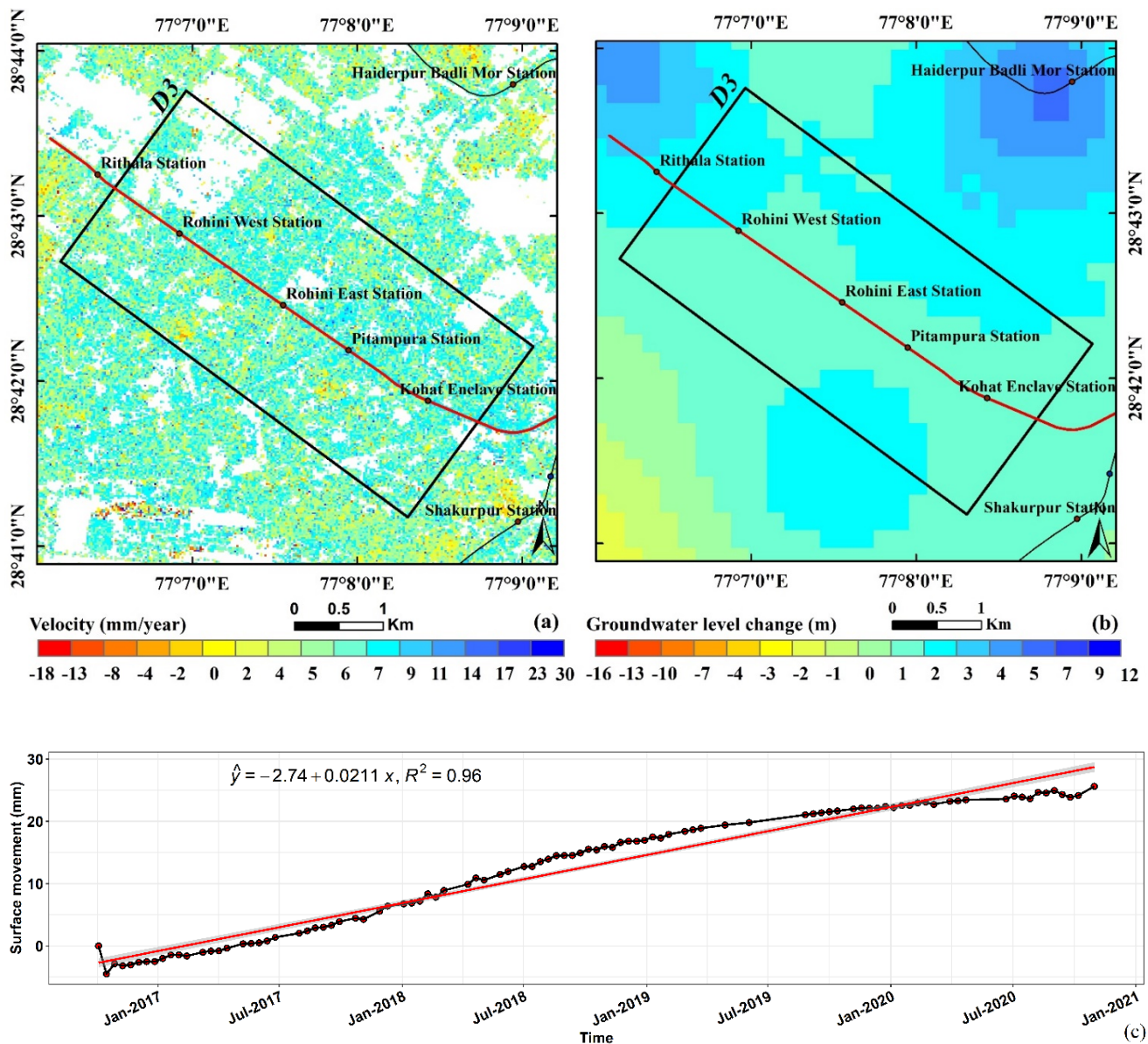


Figure 9. For Rohini PSInSAR: (a) land uplift map, (b) groundwater augmentation map, and (c) time-series of land uplift for the whole area marked in box.

5.4. Modelling of Land Deformation due to Groundwater Change

The results discussed in Sections 5.1–5.3 establish that a reduction in groundwater level can result in the compaction of strata and subsequent subsidence of the overlying terrain. Due to a change in hydrostatic pressure, the amount of compaction depends on the rock matrix's physical properties and the strata's geological setting. A mathematical model was constructed to calculate the expected land deformation owing to a given change in the groundwater level.

The model requires input parameters of the change in groundwater level, the thickness of underlying geological units, and geological characteristics (Table 2). The model is set to run for any number of time steps, the size of which are defined by the rate of piezometric head reduction. As the model time-step is advanced, it recalculates the new formation thickness, void ratio, and compaction. A monthly rate was found to be the best compromise between time and resolution. For our study, two test cases were conducted using differing temporal resolutions for the groundwater level fluctuation:

Case 1 required the model to be run using a 4-year average change in groundwater for all the locations studied above in London and NCT-Delhi. The 4-year average was divided into monthly rates for each location, and the model was run for the 4-year (48 months) duration.

Case 2 focused on a single location at Battersea Power Station, London. Here, monthly rates of head fluctuation were used, based upon levels measured at a groundwater pumping station. The model was tested only for one location in London since continuous monthly groundwater variations for other locations could not be obtained.

The results obtained from case 1 are summarised in Table 4. The difference in land-surface deformation rate calculated using the model and measured using PSInSAR varied between 0.26 and 4.83 mm/year. The correlation between both methods is shown in Figure 10. The deformation rates from both the methods have R^2 value of 0.881, indicating a very high rate of correlation, thus validating the model and PSInSAR results. It also confirms quantitatively that the observed deformation is directly associated with changes in the groundwater level

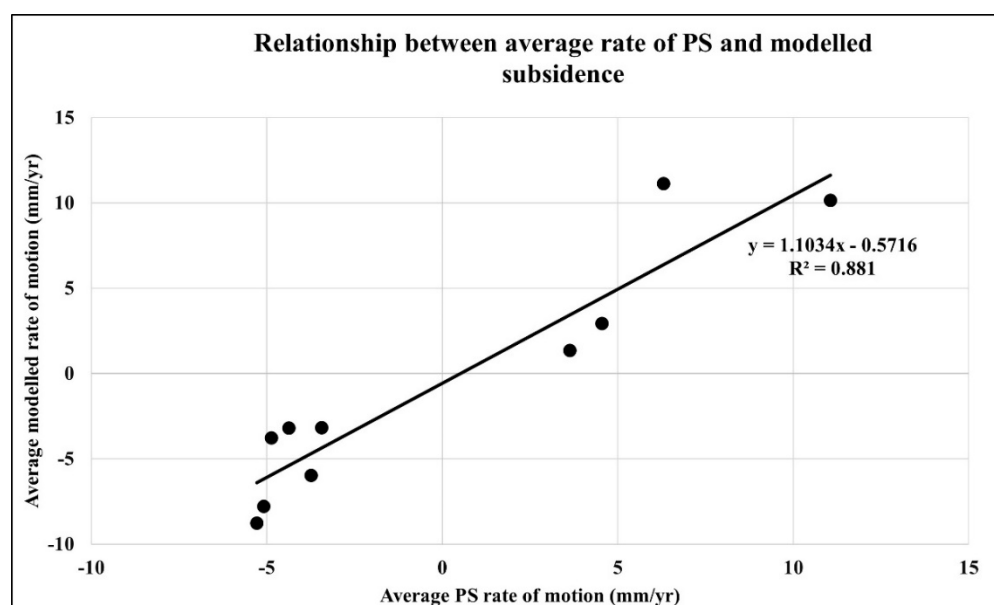


Figure 10. Correlation between the modelled and PSInSAR measured land-surface deformation.

For the Battersea case, the monthly groundwater fluctuation was obtained for 4-year period between October 2016 and November 2020. The piezometric head exhibited a constant decrease in groundwater levels. The compaction predicted by the model over the 4-year pumping period for Battersea is given in Figure 11. As no time-lag constant was used, the modelled variation in compaction rate varies considerably on a monthly scale, in-line with the groundwater levels that were input. August 2016 was used as the datum for the groundwater change and compaction rates. The land movement from two different datasets is interestingly very similar. Direct comparison of the motion rates is not possible since the dates when groundwater levels were measured and the radar scenes were acquired are not coincident. Statistically, the two datasets are very similar; the average rate of motion for the PSInSAR is -6.05 mm/year and for the modelled motions it is -5.51 mm/year, which is a difference of just 0.54 mm/year. The small difference between the modelled deformation for a given groundwater level (using either case 1 or 2) and the actual measured deformation (from PSInSAR) adds confidence to the argument that the observed motion is indeed primarily associated with the groundwater change.

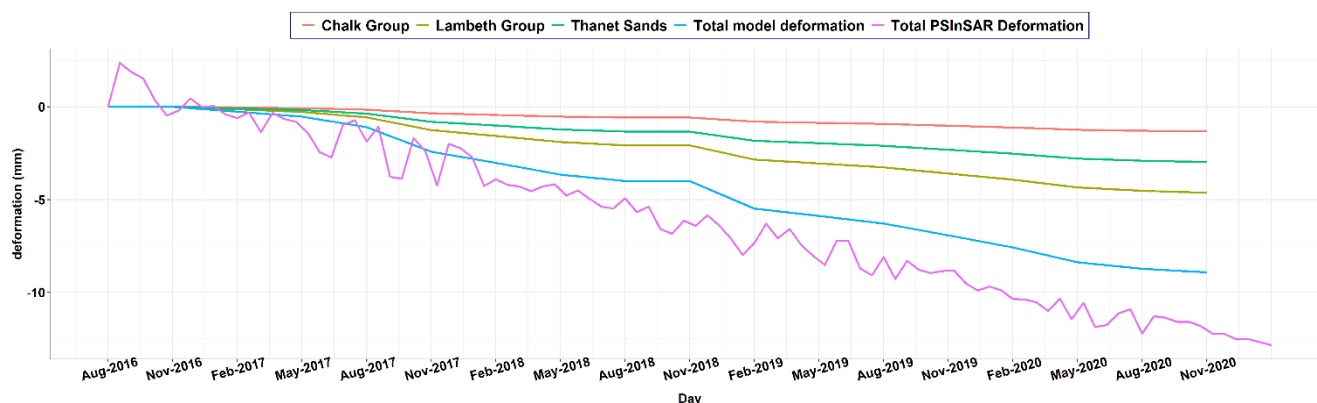


Figure 11. Time series for modelled and PSInSAR measured land-surface deformation for Battersea, London.

6. Conclusions

In this study, we examined the land movement pattern for London and NCT-Delhi during 2016–2020 using the PSInSAR methodology, and sought to establish the factors governing this land movement. Both cities were found to have experienced long-term, complex, non-uniform patterns of land motion in the spatial and temporal domains. We analysed different types of site-specific movement of uplift, subsidence, and differential motion, along with the corresponding groundwater variations. Across both the cities and all types of movement, the most common factor controlling the spatial patterns of land motion was the change in groundwater level. It can be concluded that when groundwater is extracted from an aquifer, it leads to land subsidence. Conversely, a rebound or recharge of groundwater leads to land uplift. NCT-Delhi has been declared as a groundwater critical zone by the government of India. It is one of the most exploited cities with regards to groundwater owing to its urban fabric and ever-increasing population, and these results offer confirmation of that. London is not recognised by a critical status, but its ever-increasing population and government's aquifer recharge policy exerts local pressure and this is borne out by results shown for areas L1-a and L2. Along with the groundwater extraction and recharge, sub-surface geology, underground construction, and metro extensions all contribute to form a complex land movement pattern.

The results obtained from the mathematical model agree well with our PSInSAR results. The formations are considered homogeneous, and the water removal is considered as a rate of piezometric head reduction (m/time) and not a quantity removed (m^3), and the time-lag constant was not considered in the model. It is however possible to apply the time-lag constant to the output after the model if an approximation of the time-lag is required. The accuracy of the model relies on the accuracy of the groundwater level input, and with actual observed groundwater data, the model could be verified for other locations as well. Since, the model is able to estimate the land-surface deformation rate and pattern for a known groundwater level change, it could be useful for assessing and mitigating risks associated with ground deformation.

Whilst the two cities are superficially different in terms of civil engineering, the response of their groundwater to engineering decisions (such as underground metro construction) and how that is reflected in change in surface-level tells a similar story. This suggests that it may be a universal effect, which we might anticipate observing in other major cities worldwide, which are subjected to similar engineering decisions. Some InSAR deformation relating to groundwater results have been presented before for London, but not in NCT-Delhi. The purpose of the paper was to demonstrate that a groundwater and subsidence inter-relationship generally holds true. This study can serve as a guideline to government agencies in identifying the areas and extent of groundwater-induced land subsidence, and to take proper steps to mitigate them.

Author Contributions: Conceptualization, V.A., R.L.G., and S.M.; data curation, V.A., A.K., and S.M.; formal analysis, V.A., A.K., D.G., S.G., R.L.G., and S.M.; funding acquisition, V.A.; investigation, V.A., A.K., S.G., R.L.G., and S.M.; methodology, V.A., A.K., D.G., S.G., R.L.G., and S.M.; resources, V.A.; software, V.A., and S.M.; supervision, R.L.G. and S.M.; validation, V.A., S.G., and S.M.; visualization, V.A. and S.M.; writing—original draft, V.A.; writing—review and editing, A.K., D.G., S.G., R.L.G., and S.M. All authors have read and agreed to the published version of the manuscript.

Funding: The research was funded by the University of Nottingham Faculty of Engineering Research Excellence PhD scholarship.

Acknowledgments: The authors would like to thank the European Space Agency (ESA) for providing access to SARscape software for the processing of InSAR data through Eohops programme. We would also like to thank the Environment Agency for providing the “management of the London basin chalk aquifer” status reports.

Conflicts of Interest: The authors declare no conflict of interest.

References

- Dalin, C.; Wada, Y.; Kastner, T.; Puma, Y.W.M.J. Groundwater depletion embedded in international food trade. *Nature* **2017**, *543*, 700–704.
- Wada, Y.; Van Beek, L.P.H.; Van Kempen, C.M.; Reckman, J.W.T.M.; Vasak, S.; Bierkens, M.F.P. Global depletion of groundwater resources. *Geophys. Res. Lett.* **2010**, *37*, 37.
- Konikow, L.F.; Kendy, E. Groundwater depletion: A global problem. *Hydrogeol. J.* **2005**, *13*, 317–320.
- Li, M.-G.; Chen, J.-J.; Xu, Y.-S.; Tong, D.-G.; Cao, W.-W.; Shi, Y.-J. Effects of groundwater exploitation and recharge on land subsidence and infrastructure settlement patterns in Shanghai. *Eng. Geol.* **2021**, *282*, 105995.
- Figueroa-Miranda, S.; Vargas, J.T.; Ramos-Leal, J.A.; Madrigal, V.M.H.; Villaseñor-Reyes, C.I. Land subsidence by groundwater over-exploitation from aquifers in tectonic valleys of Central Mexico: A review. *Eng. Geol.* **2018**, *246*, 91–106.
- Zhang, Y.-Q.; Wang, J.-H.; Li, M.-G. Effect of dewatering in a confined aquifer on ground settlement in deep excavations. *Int. J. Géoméch.* **2018**, *18*, 04018120.
- Zheng, G.; Ha, D.; Zeng, C.; Cheng, X.; Zhou, H.; Cao, J. Influence of the opening timing of recharge wells on settlement caused by dewatering in excavations. *J. Hydrol.* **2019**, *573*, 534–545.
- Lyu, H.-M.; Shen, S.-L.; Zhou, A.; Yang, J. Risk assessment of mega-city infrastructures related to land subsidence using improved trapezoidal FAHP. *Sci. Total Environ.* **2020**, *717*, 135310.
- Chai, J.C.; Shen, S.L.; Zhu, H.H.; Zhang, X.L. Land subsidence due to groundwater drawdown in Shanghai. *Geotechnique* **2004**, *54*, 143–147.
- Bateson, L.B.; Barkwith AK, A.P.; Hughes, A.G.; Aldiss, D.T. Terrafirma: London H-3 modelled product: Comparison of PS data with the results of a groundwater abstraction related subsidence model. *Br. Geol. Surv. Comm. Rep.* **2009**, *32*, 4–47. Available online: <http://nora.nerc.ac.uk/id/eprint/8581/1/OR09032.pdf> (accessed on 12 July 2021).
- Yu, H.; Gong, H.; Chen, B.; Liu, K.; Gao, M. Analysis of the influence of groundwater on land subsidence in Beijing based on the geographical weighted regression (GWR) model. *Sci. Total Environ.* **2020**, *738*, 139405, doi:10.1016/j.scitotenv.2020.139405.
- Galloway, D.L.; Burbey, T.J. Review: Regional land subsidence accompanying groundwater extraction. *Hydrogeol. J.* **2011**, *19*, 1459–1486.
- Scoular, J.; Ghail, R.; Mason, P.J.; Lawrence, J.; Bellhouse, M.; Holley, R.; Morgan, T. Retrospective InSAR analysis of east London during the construction of the Lee tunnel. *Remote Sens.* **2020**, *12*, 849.
- Agarwal, V.; Kumar, A.; Gomes, R.L.; Marsh, S. Monitoring of ground movement and groundwater changes in London using InSAR and GRACE. *Appl. Sci.* **2020**, *10*, 8599, doi:10.3390/app10238599.
- Biswas, K.; Chakravarty, D.; Mitra, P.; Misra, A. Spatial-correlation based persistent scatterer interferometric study for ground deformation. *J. Indian Soc. Remote Sens.* **2017**, *45*, 913–926, doi:10.1007/s12524-016-0647-5.
- Peltier, A.; Bianchi, M.; Kaminski, E.; Komorowski, J.-C.; Rucci, A.; Staudacher, T. PSInSAR as a new tool to monitor pre-eruptive volcano ground deformation: Validation using GPS measurements on Piton de la Fournaise. *Geophys. Res. Lett.* **2010**, *37*, doi:10.1029/2010gl043846.
- Kim, J.-S.; Kim, D.-J.; Kim, S.-W.; Won, J.-S.; Moon, W.M. Monitoring of urban land surface subsidence using PSInSAR. *Geosci. J.* **2007**, *11*, 59–73, doi:10.1007/bf02910381.
- Karanam, V.; Motagh, M.; Garg, S.; Jain, K. Multi-sensor remote sensing analysis of coal fire induced land subsidence in Jharia Coalfields, Jharkhand, India. *Int. J. Appl. Earth Obs. Geoinf.* **2021**, *102*, 102439, doi:10.1016/j.jag.2021.102439.
- Ferretti, A.; Prati, C.; Rocca, F. Nonlinear subsidence rate estimation using permanent scatterers in differential SAR interferometry. *IEEE Trans. Geosci. Remote Sens.* **2000**, *38*, 2202–2212, doi:10.1109/36.868878.
- Mason, P.J.; Ghail, R.C.; Bischoff, C.; Skipper, J.A. *Detecting and Monitoring Small-Scale Discrete Ground Movements Across London, Using Persistent SCATTERER InSAR (PSI)*; ICE Publishing: London, UK, 2015.

21. Khorrami, M.; Alizadeh, B.; Tousi, E.G.; Shakerian, M.; Maghsoudi, Y.; Rahgozar, P. How groundwater level fluctuations and geotechnical properties lead to asymmetric subsidence: A PSInSAR Analysis of land deformation over a transit corridor in the Los Angeles Metropolitan area. *Remote Sens.* **2019**, *11*, 377.
22. Khorrami, M.; Abrishami, S.; Maghsoudi, Y.; Alizadeh, B.; Perissin, D. Extreme subsidence in a populated city (Mashhad) detected by PSInSAR considering groundwater withdrawal and geotechnical properties. *Sci. Rep.* **2020**, *10*, 1–16.
23. Devleeschouwer, X.; Declercq, P.Y.; Flamion, B.; Brixko, J.; Timmermans, A.; Vanneste, J. Uplift revealed by radar interferometry around Liège (Belgium): A relation with rising mining groundwater. In Proceedings of the Post-Mining Symposium, Nancy, France, 6–8 February 2008; pp. 6–8.
24. Jones, M.A.; Hughes, A.; Jackson, C.; Van Wonderen, J.J. Groundwater resource modelling for public water supply management in London. *Geol. Soc. Lond. Spéc. Publ.* **2012**, *364*, 99–111, doi:10.1144/sp364.8.
25. EA. *Management of the London Basin Chalk Aquifer*. Environment Agency: Bristol, UK, 2019.
26. Central Ground Water Board. *Ground Water Year Book-India 2017–2018*; Ministry of Water Resources, River Development and Ganga Rejuvenation: New Delhi, India, 2018.
27. Central Ground Water Board. *Ground Water Year Book, NCT Delhi, 2015–2016*; Central Ground Water Board: Kolkata, India, 2016.
28. Gupte, P.R. *Groundwater Resources vs Domestic Water Demand and Supply-NCT Delhi*; Central Ground Water Board: Kolkata, India, 2019.
29. Garg, S.; Motagh, M.; Jayaluxmi, I. Land Subsidence in Delhi, India investigated using Sentinel-1 InSAR measurements. In Proceedings of the EGU General Assembly 2020, Online, 4–8 May 2020; <https://doi.org/10.5194/egusphere-egu2020-21138>.
30. Ford, J.R.; Mathers, S.J.; Royse, K.; Aldiss, D.T.; Morgan, D.J. Geological 3D modelling: Scientific discovery and enhanced understanding of the subsurface, with examples from the UK. *Z. Dtsch. Ges. Für Geowiss.* **2010**, *161*, 205–218, doi:10.1127/1860-1804/2010/0161-0205.
31. Mathers, S.; Burke, H.; Terrington, R.; Thorpe, S.; Dearden, R.; Williamson, J.; Ford, J. A geological model of London and the Thames Valley, southeast England. *Proc. Geol. Assoc.* **2014**, *125*, 373–382, <https://doi.org/10.1016/j.pgeola.2014.09.001>.
32. BGS. *Industrial and Urban Pollution of Groundwater*; UK Groundwater Forum: Oxfordshire, UK, 2013.
33. Boni, R.; Cigna, F.; Bricker, S.; Meisina, C.; McCormack, H. Characterisation of hydraulic head changes and aquifer properties in the London Basin using Persistent Scatterer Interferometry ground motion data. *J. Hydrol.* **2016**, *540*, 835–849, doi:10.1016/j.jhydrol.2016.06.068.
34. Central Ground Water Board. *Groundwater Scenario in India, November 2016*; Central Ground Water Board: Kolkata, India, 2016.
35. GLA. London Datastore. Greater London Authority (GLA). 2021. Available online: <https://data.london.gov.uk/dataset/trend-based-population-projections> (accessed on: 12 July 2021).
36. ESD. Demographic Profile of Delhi, Economic SURVEY of Delhi. 2021. Available online: http://delhiplanning.nic.in/sites/default/files/19_Demography.pdf (accessed on: 12 July 2021).
37. PS Tutorial. Sarmap SA, Switzerland. 2014. Available online: http://www.sarmap.ch/tutorials/PS_Tutorial_V_0_9.pdf (accessed on 12 July 2021).
38. Agarwal, V.; Kumar, A.; Gomes, R.L.; Marsh, S. An overview of SAR sensors and software and a comparative study of open source (Snap) and commercial (SARscape) software for DInSAR analysis using C-band Radar images. In Proceedings of the 41st Asian Conference on Remote Sensing—ACRS, Deqing, China, 9–11 November 2020. Available online: <https://www.researchgate.net/publication/345335178> (accessed on: 15 May 2021).
39. Simonetto, E.; Follin, J.-M. An overview on interferometric SAR software and a comparison between DORIS and SARSCAPE Packages. In *Lecture Notes in Geoinformation and Cartography*; Springer: New York, NY, USA, 2012.
40. Sahraoui, O.H.; Hassaine, B.; Serief, C. Radar Interferometry with Sarscape Software. In Proceedings of the XXIII FIG Congress Munich, Germany, 8–13 October 2006.
41. Sarmap. SARscape Help Manual. 2014. Available online: <http://sarmap.ch/tutorials/Basic.pdf> (accessed on 12 July 2021).
42. EA. *Management of the London Basin Chalk Aquifer*. Status Report 2017; Environ. Agency: Bristol, UK, 2017. Available online: <https://www.gov.uk/government/publications/london-basin-chalk-aquifer-annual-status-report> (accessed on 12 July 2021).
43. Bartier, P.M.; Keller, C. Multivariate interpolation to incorporate thematic surface data using inverse distance weighting (IDW). *Comput. Geosci.* **1996**, *22*, 795–799, doi:10.1016/0098-3004(96)00021-0.
44. Gee, D.; Bateson, L.; Grebby, S.; Novellino, A.; Sowter, A.; Wyatt, L.; Marsh, S.; Morgenstern, R.; Athab, A. Modelling groundwater rebound in recently abandoned coalfields using DInSAR. *Remote Sens. Environ.* **2020**, *249*, 112021. doi:10.1016/j.rse.2020.112021.
45. Terzaghi, K. Principles of soil mechanics, IV—Settlement and consolidation of clay. *Eng. News-Rec.* **1925**, *95*, 874–878.
46. Shearer, T. A numerical model to calculate land subsidence, applied at Hangu in China. *Eng. Geol.* **1998**, *49*, 85–93.
47. Poland, J.F. Guidebook to studies of land subsidence due to ground-water withdrawal; UNESCO: Paris, France, 1984.
48. Zimmerman, R.W. *Compressibility of Sandstones*; Elsevier: Amsterdam, The Netherlands, 1990.
49. Sarkar, A.; Ali, S.; Kumar, S.; Shekhar, S.; Rao, S. Groundwater environment in Delhi, India. In *Groundwater Environment in Asian Cities*; Elsevier: Amsterdam, The Netherlands, 2016; pp. 77–108.
50. Zheng, M.; Deng, K.; Fan, H.; Du, S. Monitoring and analysis of surface deformation in mining area based on InSAR and GRACE. *Remote Sens.* **2018**, *10*, 1392, doi:10.3390/rs10091392.
51. Transport for London, Northern Line Extension—Transport for London. 2021. Available online: <https://tfl.gov.uk/travel-information/improvements-and-projects/northern-line-extension> (accessed on 4 April 2021).

52. DMRC. Delhi Metro Present Projects (DMRC), DMRC Off. Website. 2021. Available online: <http://www.delhimetrorail.com/projectpresent.aspx> (accessed on 21 July 2021).
53. DMRC. Annual Report of DMRC 2017–2018. 2018. Available online: http://www.delhimetrorail.com/annual_report.aspx/ (accessed on).
54. BGS. Geindex Onshore for Boreholes Provided by British Geological Survey. 2021. Available online: <http://mapapps2.bgs.ac.uk/geindex/home.html?layer=BGSBoreholes> (accessed on 5 May 2021).
55. Aldiss, D. *The Stratigraphical Framework for the Palaeogene Successions of the London Basin, UK*; British Geography Survey: Nottingham, UK, 2014.
56. Geoiq. GeoIQ's Spatial AI: India's Comprehensive and Granular Location Data Stack, Geoiq. 2021. Available online: <https://geoiq.io/> (accessed on 2 April 2021).
57. E.P. 7. 3. 3. 778. Google, Delhi Haryana Border. 28°30'54.84" N, 77° 4'21.80" E, Eye alt 13.45 km. Borders and labels; Places Layers. NOAA, DigitalGlobe 2021, Google Earth. Available online: <http://www.google.com/earth/index.html> (accessed on 10 July 2021).
58. Mammen, S.S. Delhi's Most Expensive and Posh Residential Areas. Available online: <https://housing.com/news/posh-residential-areas-in-delhi/> (accessed on 20 September 2021).